Uniosun Journal of Engineering and Environmental Sciences (UJEES), Vol. 8 No. 2, Sept., 2026
DOI: 10.64980/ujees.v8i2.030 **Aminu and Adebayo**
Published: September 30, 2026

OPTIMAL PLACEMENT OF PHOTOVOLTAIC AND WIND GENERATION UNITS FOR VOLTAGE STABILITY ENHANCEMENT IN POWER SYSTEMS USING THE MAYFLY OPTIMIZATION ALGORITHM

Isiaka Olatunde AMINU[1] and Isaiah Gbadegesin ADEBAYO[2*]

[1,2]*Department of Electronic and Electrical Engineering, Ladoke Akintola University of Technology, P.M.B, 4000, Ogbomoso, Nigeria.*

[*]*Corresponding Author: igadebayo@lautech.edu.ng*

Abstract
This study presents a Mayfly Optimization Algorithm (MOA)-based approach for voltage stability enhancement and optimal integration of renewable energy resources in the IEEE 30-bus transmission system under steady state contingency conditions. The methodology combines Newton-Raphson load flow analysis, Bus Voltage Stability Index (BVSI), and MOA to identify the most vulnerable buses and determine suitable locations for photovoltaic (PV) and wind generator installation. Contingency scenario was created by increasing the reactive load demand across the network, resulting in significant voltage degradation and increased system losses. The MOA based BVSI was then applied to identify critical buses requiring corrective actions. Simulation results revealed that buses 5, 16, and 23 were the weakest buses with the highest fitness values and therefore selected for renewable energy integration. Under contingency conditions, active and reactive power losses increased from 324.31 MW and 228.85 MVAr to 453.06 MW and 329.85 MVAr, respectively. Application of MOA reduced these losses to 338.10 MW and 257.60 MVAr. Further integration of optimally sized PV and wind generators significantly improved voltage profiles and reduced active power losses to 256.40 MW and 283.77 MW, respectively. Comparative analysis showed that the proposed BVSI-MOA approach outperformed the Equilibrium Optimizer (EO) and Line Stability Index (LSI) methods in identifying critical buses and minimizing system losses. The results demonstrate the effectiveness of MOA-based renewable energy integration for improving voltage stability, reducing transmission losses, and enhancing overall power system performance.

Keywords
Mayfly Optimization Algorithm, Voltage Stability, Renewable Energy Integration, Photovoltaic Generator, Wind Generator, IEEE 30-Bus System, Contingency Analysis, Power Loss Reduction.

1. INTRODUCTION

The increasing global demand for electrical energy, coupled with environmental concerns associated with fossil-fuel-based electricity generation, has accelerated the deployment of Renewable Energy Sources (RESs) in modern power systems. Solar photovoltaic (PV) and wind energy technologies have emerged as the most promising renewable energy alternatives due to their environmental sustainability, technological maturity, and declining installation costs [1,2]. The integration of these renewable energy resources into transmission networks offers significant benefits, including reduced greenhouse gas emissions, enhanced energy security, and diversification of generation portfolios. However, the intermittent and stochastic nature of solar and wind resources introduces operational challenges that may adversely affect power system stability, voltage regulation, and overall network reliability [3-5]. Voltage stability has become one of the major concerns in contemporary power system planning and operation. It refers to the capability of a power system to maintain acceptable voltage levels at all buses during normal operating conditions and after being subjected to disturbances [6]. Rapid load growth, increased power transfer across transmission corridors, and inadequate reactive power support has heightened the risk of voltage instability and voltage collapse in many power networks worldwide [4, 7, 8]. The integration of renewable energy sources without proper planning may further aggravate these challenges due to their variable output characteristics and dependence on weather conditions. Consequently, identifying optimal locations for renewable energy integration has become an essential requirement for maintaining system stability and improving network performance [9-12]. Numerous studies have investigated the optimal placement of renewable energy resources and distributed generation units within power systems. Conventional optimization techniques such as linear programming, nonlinear programming, and mixed-integer programming have been applied to solve renewable energy allocation problems. However, the highly nonlinear and non-convex nature of power system optimization problems

often limits the effectiveness of these traditional approaches [13-16]. To overcome these limitations, various metaheuristic optimization algorithms, including Genetic Algorithm (GA), Particle Swarm Optimization (PSO), Grey Wolf Optimizer (GWO), Whale Optimization Algorithm (WOA), and Equilibrium Optimizer (EO), have been employed for optimal renewable energy integration and voltage stability enhancement [17-23]. Although these algorithms have demonstrated satisfactory performance, challenges associated with premature convergence, local optimum entrapment, and computational complexity still exist [24-30]. Recently, the Mayfly Optimization Algorithm (MOA) has gained considerable attention due to its excellent balance between exploration and exploitation capabilities. MOA is a population-based optimization technique inspired by the mating behavior and flight movement of mayflies. The algorithm combines the advantages of swarm intelligence and evolutionary optimization mechanisms to achieve efficient global and local search capabilities. Its ability to avoid local optima and achieve faster convergence makes it particularly suitable for solving complex engineering optimization problems, including power system planning and renewable energy integration studies [10, 31, 32]. The IEEE 30-bus transmission system is widely recognized as a standard benchmark network for evaluating optimization techniques and power system analysis methodologies. The system consists of multiple generation units, load buses, and transmission lines that adequately represent the operational characteristics of practical transmission networks. By optimally locating solar PV and wind generation units within the IEEE 30-bus system, significant improvements can be achieved in voltage profile enhancement, transmission loss reduction, and voltage stability margin improvement while satisfying operational constraints [12,13]. This study therefore presents a MOA-based framework for the optimal placement of photovoltaic and wind generation units in the IEEE 30-bus transmission system. Newton-Raphson load flow analysis is employed to evaluate the steady-state operating conditions of the network, while voltage stability indices are utilized to identify critical buses and assess system stability performance. The proposed optimization framework aims to determine the most suitable renewable energy installation locations that minimize transmission losses, improve voltage profiles, and enhance overall voltage stability. The effectiveness of the proposed method is validated through simulation studies and comparative performance assessment with established optimization techniques. The outcomes of this research are expected to provide useful insights for power system planners and operators seeking to maximize the benefits of renewable energy integration while maintaining secure and reliable network operation.

Thus, the major contributions of this study are highlighted as follows.

i. Development of a Mayfly Optimization Algorithm (MOA)-based framework that integrates Bus Voltage Stability Index (BVSI) assessment for identifying critical buses and determining the optimal placement of solar PV and wind generation units in the IEEE 30-bus transmission system.
ii. Development of a unified framework that combines voltage-stability-based critical-bus identification with renewable-energy allocation and optimisation under contingency conditions, with the objective of improving voltage profiles and reducing transmission losses.
iii. A comparative assessment of the proposed BVSI-MOA framework with the Line Stability Index (LSI) and Equilibrium Optimizer (EO), using critical-bus identification, voltage magnitude and active power loss as performance indicators under the same network operating and contingency conditions.

The integration of RES into power transmission systems has attracted significant research attention due to the growing need for sustainable electricity generation and improved power system performance. Researchers have investigated various approaches for the optimal placement and sizing of RES with the objectives of minimizing transmission losses, improving voltage profiles, enhancing voltage stability, and reducing operational costs. Mayfly Optimization Algorithm (MOA) is a nature-inspired metaheuristic optimisation technique introduced in [31], which mimics the mating behaviour and flight dynamics of mayflies. The algorithm was evaluated using several benchmark optimization functions and demonstrated superior convergence characteristics compared with Particle Swarm Optimization (PSO), Genetic Algorithm (GA), and Firefly Algorithm (FA). The study concluded that MOA possesses a strong balance between exploration and exploitation capabilities, making it suitable for solving complex engineering optimization problems. However, the work was limited to mathematical benchmark functions and did not investigate power system applications. The Equilibrium Optimizer (EO) developed in [14], is a physics-inspired metaheuristic optimisation algorithm that emulates the dynamic mass balance process used to describe the movement of mass towards an equilibrium state. The algorithm was validated using several unconstrained and constrained optimization problems and showed competitive performance compared with established optimization techniques. The authors reported that EO effectively avoids local optima while maintaining a high convergence rate. Despite its effectiveness, the algorithm was not specifically designed for renewable energy allocation or voltage stability enhancement in transmission networks. Particle Swarm Optimisation (PSO) was applied in [2] to determine the optimal placement and sizing of distributed generation (DG) units in electrical power systems. The objective was to minimize power losses and improve voltage profiles. Simulation results revealed significant reductions in real power losses and improvements in voltage magnitude across the network. Nevertheless, the algorithm exhibited sensitivity to parameter tuning and

occasionally suffered from premature convergence when solving large-scale optimization problems. Whale Optimization Algorithm (WOA) was investigated in [21] for optimal allocation of wind generation units. The objective function incorporated power loss minimization and voltage profile enhancement under various loading conditions. The results indicated that the algorithm successfully identified suitable locations for wind generation integration and improved overall system performance. However, the study considered only wind energy resources and did not evaluate the combined effects of solar photovoltaic and wind generation integration. Author in [22] presented a hybrid Genetic Algorithm–Particle Swarm Optimization approach for renewable energy allocation in transmission networks. The hybrid technique combined the global search capability of GA with the fast convergence characteristics of PSO. The results demonstrated better optimization performance than the individual algorithms. Despite these improvements, the computational burden increased significantly due to the hybridization process, making real-time implementation more challenging. The performance of the Mayfly Optimization Algorithm was evaluated in [28] to solve various engineering design optimization problems. Their findings indicated that MOA achieved higher optimization accuracy and faster convergence rates than several well-established metaheuristic algorithms. The authors attributed the superior performance to the mating and mutation mechanisms embedded within the algorithm. However, the study did not consider renewable energy integration or power system stability applications. Improve MOA was applied in [18] to optimal power flow problems and reported significant reductions in transmission losses and generation costs. The algorithm demonstrated effective handling of nonlinear constraints and achieved superior performance compared with conventional optimization approaches. Although the study highlighted the suitability of MOA for power system optimization, renewable energy placement and voltage stability assessment were not incorporated into the optimization framework. Voltage stability assessment was investigated in [3] using voltage stability indices for transmission network analysis. The study demonstrated that indices such as Fast Voltage Stability Index (FVSI), Line Stability Index (LSI), Voltage Collapse Point Indicator (VCPI), and Voltage Deviation Index (VDI) are effective tools for identifying critical buses and transmission lines that are susceptible to voltage instability. The authors emphasized that these indices provide useful information for preventive control and system planning. However, optimization-based renewable energy integration strategies were not considered. Application of voltage stability indices was examined in [26] for identifying weak buses in transmission networks. The study revealed that buses with higher stability index values are more vulnerable to voltage collapse and require corrective measures such as reactive power compensation. The authors recommended the integration of optimization algorithms with voltage stability assessment techniques to achieve improved system performance. Recent studies have increasingly focused on combining renewable energy integration with advanced optimization techniques to improve power system stability. Author in [1] demonstrated that modern metaheuristic algorithms provide efficient solutions for highly nonlinear optimization problems in power systems. Similarly, [7] reported that MOA possesses superior exploration capability, improved convergence characteristics, and better avoidance of local optima compared with several existing optimization techniques. These characteristics suggest that MOA has significant potential for solving renewable energy placement problems aimed at voltage stability enhancement. Although substantial research has been conducted on renewable energy integration, voltage stability assessment, and optimization-based power system planning, several gaps remain in the existing literature. Many studies focus on either renewable energy allocation or voltage stability enhancement independently, while relatively few investigations integrate both objectives within a unified optimization framework. Furthermore, limited studies have explored the application of the MOA for simultaneous placement of solar photovoltaic and wind generation units with explicit consideration of voltage stability indices. Therefore, this study presents a MOA-based optimization framework for the optimal placement of solar PV and wind generation units in the IEEE 30-bus transmission system with the aim of minimizing transmission losses, improving voltage profiles, and enhancing voltage stability margins.

2. MATERIALS AND METHOD

In this study, the optimal placement and sizing of solar PV and wind generation units in the IEEE 30-bus transmission system were formulated as an optimisation problem and embedded directly within the MOA. The Bus Voltage Stability Index (BVSI) and voltage profile obtained from Newton-Raphson (NR) load-flow analysis were incorporated into the optimisation process to guide the identification of voltage-sensitive buses. MOA simultaneously determines the locations and capacities of the PV and wind generation units by searching for the solution that minimises the defined objective function while satisfying the specified network operating constraints. The optimisation objective considers voltage stability improvement, voltage deviation and active power loss, subject to bus voltage, generator output and transmission-line thermal limits, The simulation of the approaches were carried out using MATLABR2023a. A base-case load flow analysis was performed to determine the voltage magnitudes, voltage angles, active power losses, and reactive power losses of the network under normal operating conditions. Thereafter, voltage stability indices were computed to identify critical buses. Then MOA was subsequently employed to determine the optimal placement and sizing of solar PV and wind generation units while satisfying network operational constraints such as bus

voltage limits, generator output limits, and transmission line thermal limits. The performance of the optimization framework was evaluated by comparing the network operating conditions before and after renewable energy integration. Key performance indicators considered in the assessment include total real power loss, voltage deviation index, minimum bus voltage magnitude, voltage stability index values, convergence characteristics, and computational efficiency. The obtained results were further compared with those achieved using Line Stability Index (LSI) and the Equilibrium Optimizer (EO) to demonstrate the effectiveness and superiority of the MOA-based approach.

2.1 Description of the IEE 30-Bus Test System

The IEEE 30-bus system is one of the most widely used benchmark power networks for testing optimization algorithms, load flow techniques, voltage stability assessment methods, and renewable energy integration strategies due to its moderate complexity and realistic operational characteristics [17, 23]. The network consists of 30 buses interconnected through 41 transmission lines and transformers as shown in Figure 1. It contains six generation buses, twenty-four load buses, and four transformer tap-changing branches. The generating units are located at buses 1, 2, 5, 8, 11, and 13, while the remaining buses serve as load buses with varying active and reactive power demands. Bus 1 operates as the slack (swing) bus responsible for balancing the system power mismatch, whereas buses 2, 5, 8, 11, and 13 are designated as generator (PV) buses. The remaining buses function as load (PQ) buses. The network operates at a base power of 100 MVA and nominal voltage levels ranging from 11 kV to 132 kV depending on the bus locations and transmission sections [13, 16]. The IEEE 30-Bus system was selected because it adequately represents the operational characteristics of practical transmission networks while maintaining manageable computational complexity. The system contains multiple generation sources, transmission corridors, and load centers, making it suitable for evaluating the effects of renewable energy integration on power flow distribution, transmission losses, voltage profile, and voltage stability margins [9, 12]. The summary of the system parameters and data are presented in Table 1.

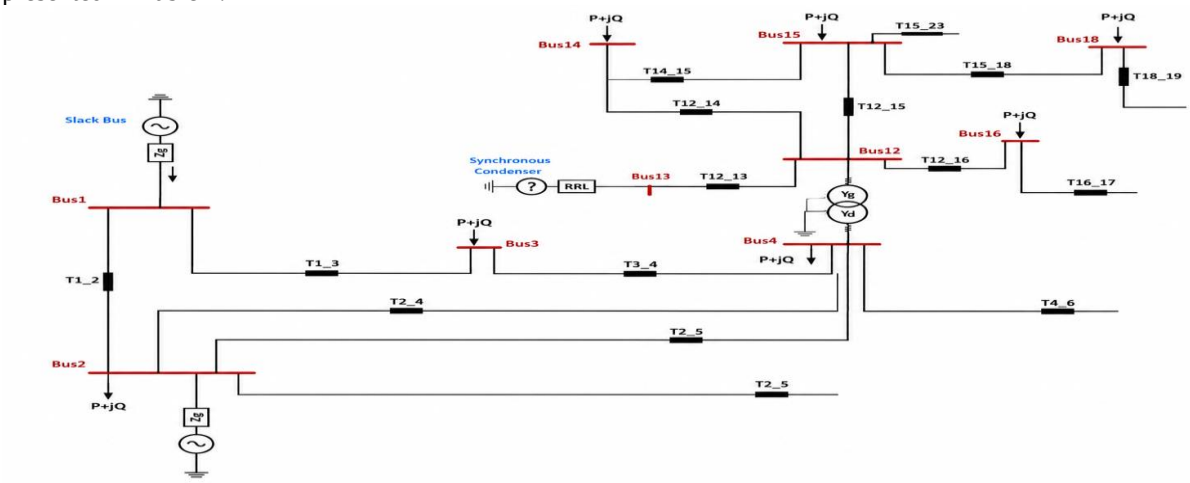


Figure 1: IEEE 30-Bus Test System

Table 1: IEEE 30-Bus System Data Summary

Parameter	Value
Number of Buses	30
Number of Generators	6
Number of Load Buses	24
Number of Transmission Lines	41
Number of Transformers	4
Slack Bus	Bus 1
PV Buses	2, 5, 8, 11, 13
PQ Buses	24
Base Power	100 MVA
Optimization Technique	Mayfly Optimization Algorithm (MOA)
Comparison Algorithm	Line Stability Index (LSI) and Equilibrium Optimizer (EO)
Load Flow Method	Newton-Raphson Method
Simulation Tool	MATLABR2023a

2.2 Newton-Raphson Load Flow Analysis

The Newton-Raphson (NR) load flow method was employed in this study to determine the steady-state operating conditions of the IEEE 30-bus transmission system before and after the integration of PV and wind generation units. The NR method is based on the iterative solution of nonlinear algebraic equations describing the relationship between bus power injections and bus voltages. For an N-bus power system, the net active and reactive power load Equations at bus i are expressed as Equations 1 and 2:

$$P_i = \sum_{j=1}^{N} |V_i||V_j||Y_{ij}|\cos\left(\theta_{ij} + \delta_j - \delta_i\right) \quad 1$$

$$Q_i = \sum_{j=1}^{N} |V_i||V_j||Y_{ij}|\sin\left(\theta_{ij} + \delta_j - \delta_i\right) \quad 2$$

where P_i and Q_i are the net active and reactive power load at bus i, V_i and V_j are the bus voltages, Y_{ij} is the admittance between buses i and j, and δ_i and δ_j are the voltage phase angles., θ_{ij} is the voltage phase angle difference between buses i and j, I_i is the injected current at bus i, N is the number of buses. The mismatch between the scheduled and calculated power values is computed at each iteration as Equations 3 and 4

$$\Delta P_i = P_i^{sch} - P_i^{cal} \quad 3$$

$$\Delta Q_i = Q_i^{sch} - Q_i^{cal} \quad 4$$

where ΔP_i and ΔQ_i are mismatch active and reactive powers at bus i, P_i^{sch} and Q_i^{sch} are the active and reactive scheduled power, P_i^{cal} and Q_i^{cal} are the active and reactive calculated power,

The objective of the iterative process is to reduce the active and reactive power mismatches until a predefined convergence tolerance is achieved. The mismatch vector (ΔS) is represented as Equation 5:

$$AS = \begin{bmatrix} \Delta P \\ \Delta Q \end{bmatrix} \quad 5$$

where ΔS is the mismatch vector , ΔP and ΔQ are mismatch active and reactive powers

The NR algorithm updates the voltage angles and voltage magnitudes using the Jacobian matrix as Equation 6:

$$\begin{bmatrix} \Delta P \\ \Delta Q \end{bmatrix} = \begin{bmatrix} J_1 & J_2 \\ J_3 & J_4 \end{bmatrix} \cdot \begin{bmatrix} \Delta\delta \\ \Delta V \end{bmatrix} \quad 6$$

where $J_1 = \frac{\partial P}{\partial \delta}$, $J_2 = \frac{\partial P}{\partial V}$, $J_3 = \frac{\partial Q}{\partial \delta}$, and $J_4 = \frac{\partial Q}{\partial V}$ are Jacobian matrix, $\Delta\delta$ is the correction in voltage angles, ΔV is the correction in voltage magnitudes, ∂P and ∂Q are derivative active and reactive power, ∂V and $\partial\delta$ are derivative voltage magnitude and angle.

The Jacobian matrix contains the partial derivatives of the active and reactive power equations with respect to voltage magnitudes and voltage angles. Solving the Jacobian matrix yields the correction vectors for voltage magnitude and phase angle updates using Equations 7 and 8:

$$\delta^{(k+1)} = \delta^{(k)} + \Delta\delta \quad 7$$

$$V^{(k+1)} = V^{(k)} + \Delta V \quad 8$$

where $V^{(k+1)}$ and $\delta^{(k+1)}$ are the updated voltage magnitude and phase angel at iteration $k+1$, $V^{(k)}$ and $\delta^{(k)}$ are the voltage magnitude and phase angel at iteration k

The iterative process continues until the maximum power mismatch satisfies as in Equation 9:

$$\max\left(|\Delta P|, |\Delta Q|\right) \leq \in \quad 9$$

where $\in$ is the convergence tolerance, typically set to 10^{-6}

Following convergence, the bus voltage profile was subsequently evaluated to identify voltage-weak buses operating outside the acceptable voltage limits, which served as a basis for voltage stability assessment as given in Equation 10:

$$0.95 p.u \leq V_i \leq 1.05 p.u \quad 10$$

The net active and reactive power generation through each transmission line from buses i to j, is subsequently determined using Equations 11 and 12:

$$P_{ij} = V_i^2 G_{ij} - V_i V_j \left[G_{ij} \cos\left(\delta_i - \delta_j\right) + B_{ij} \sin\left(\delta_i - \delta_i\right) \right] \quad 11$$

$$Q_{ij} = -V_i^2 (B_{ij} + B_{sh}) - V_i V_j \left[G_{ij} \sin\left(\delta_i - \delta_j\right) + B_{ij} \cos\left(\delta_i - \delta_i\right) \right] \quad 12$$

where P_{ij} and Q_{ij} are the net active and reactive power generation at buses i to j, B_{sh} is the line charging susceptance, B_{ij} and G_{ij} are the total line charging susceptance of the transmission line, and series reactance of the transmission line connecting buses i to j,

The active and reactive power losses were calculated using Equations 13 and 14:

$$P_{loss,ij} = P_{ij} + P_{ji} \quad 13$$

$$Q_{loss,ij} = Q_{ij} + Q_{ji} \quad 14$$

where $P_{loss,ij}$ and $Q_{loss,ij}$ are active and reactive power losses between buses i and j,

Similarly, the total active and reactive power losses were determined using Equations 15 and 16:

$$P_{loss,total} = \sum_{k=1}^{m} P_{loss,ij} \quad 15$$

$$Q_{loss,total} = \sum_{k=1}^{m} Q_{loss,ij} \quad 16$$

where $P_{loss,total}$ and $Q_{loss,total}$ are total active and reactive power loses, m is the total number of transmission lines.

The outputs obtained from the NR load flow analysis served as inputs for the computation of Bus Voltage Stability Index (BVSI), Line Stability Index (LSI), Voltage Deviation Index (VDI), and transmission power losses. These performance indicators were utilized as objective functions and evaluation criteria for determining the optimal placement and sizing of renewable energy resources within the IEEE 30-bus transmission network.

2.3 Bus Voltage Stability Index (BVSI) Formulation

In this study, the Bus Voltage Stability Index (BVSI) was employed to assess the voltage stability condition of the IEEE 30-Bus transmission system. The index provides a measure of proximity to voltage collapse by evaluating the relationship between reactive power loading and transmission line parameters [8]. The derivation of BVSI is based on the two-bus transmission line model shown in Figure 2. Considering a transmission line connecting a sending bus i and a receiving bus j, the voltage stability condition can be expressed in terms of line impedance and reactive power demand at the receiving end.

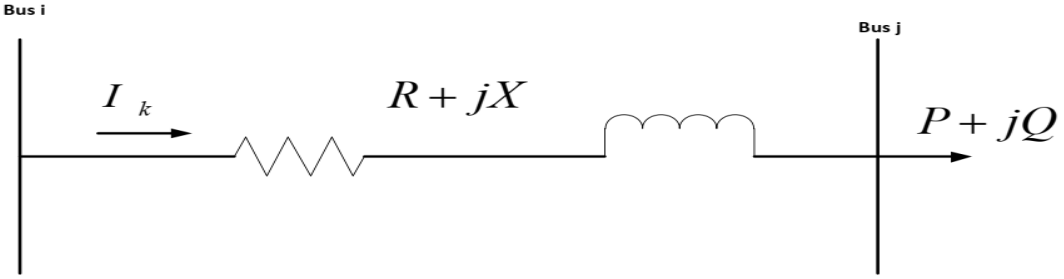


Figure 2: Single Line Diagram of Power System

The complex power equation at the receiving bus is given as Equation 17

$$S_j = P_j + jQ_j : \quad 17$$

The receiving-end current flowing into bus j is expressed as Equation 18

$$I_j = \frac{P_j - jQ_j}{V_j^*} : \quad 18$$

Using the transmission line model, the sending-end and receiving-end voltages are related by Equation 19:

$$V_i = V_j + Z_{ij} I_j \quad 19$$

Substituting the receiving-end current Equation into the voltage Equation gives Equation 20:

$$V_i = V_j + Z_{ij}\left(\frac{P_j - jQ_j}{V_j^*}\right) \quad 20$$

where V_i and V_j are the sending-end and receiving-end voltages respectively, Z_{ij} is the transmission line impedance between buses i and j, while P_j and Q_j represent the active and reactive power demands at the receiving bus, S_j is the complex apparent power, I_j is the current at receiving-end.

The NR method was employed to iteratively solve the voltage magnitudes in Equation 20. The update Equations at each iteration is: given in Jacobian as in Equation 21

$$\Delta X = -\begin{bmatrix} \frac{\partial P}{\partial \delta} & \frac{\partial P}{\partial V} \\ \frac{\partial Q}{\partial \delta} & \frac{\partial Q}{\partial V} \end{bmatrix}^{-1} F(X) \quad 21$$

where; X is the vector of unknowns voltage magnitude and angles, $F(X)$ is the vector of power mismatches. The voltage collapse occurs when: $\det(J) = 0$, or when the smallest eigenvalue approaches zero.

The new estimates bus voltages of the power system was computed as the inverse of the change in reactive power at the bus as a function of the change in voltage as given in Equation 22.

$$V_{ii+1} = \frac{1}{\left|\frac{\partial Q_i}{\partial V_i}\right|} \quad 22$$

where; $\frac{\partial Q_i}{\partial V_i}$ is the partial derivative of the reactive power Q_i with respect to the voltage magnitude V_i which can be compute from the Jacobian matrix of the power flow equations.

The partial derivative of the element of the Jacobian matrix, which describes the sensitivity of reactive power at bus i to a change in the voltage magnitude is given in Equation 23:

$$\frac{\partial Q_i}{\partial V_i} = J_{Q_i,V_i} \quad 23$$

Thus, the BVSI for bus i is expressed as in Equation 24.

$$BVSI = \frac{1}{\left|J_{Q_i,V_i}\right|} \quad 24$$

where; J_{Q_i,V_i} is the element of the Jacobian matrix J_1, J_2, J_3, J_4 .

The BVSI value ranges between 0 and 1 under stable operating conditions. As the system approaches voltage collapse, the index approaches unity as shown in Equation 25.

$$0 \le BVSI \le 1 \quad 25$$

In which:

$$BVSA \to 1$$

Therefore, transmission buses with BVSI values closest to 1 are considered the most critical and require corrective measures to improve system security. The voltage stability condition is interpreted as presented in Table 2:

Table 2: BVSI Condition

BVSI Value	System Condition
BVSI < 0.50	Stable Operating Condition
0.50 ≤ BVSI < 0.90	Moderate Voltage Stress
0.90 ≤ BVSI < 1.00	Critical Operating Condition
BVSI ≥ 1.00	Voltage Collapse Point

The BVSI values of all transmission buses in the IEEE 30-bus system were computed using the results obtained from the NR load flow analysis. The buses exhibiting the highest BVSI value were considered weak buses and selected as candidate locations for renewable energy placement.
In addition to BVSI, the Voltage Deviation Index (VDI) was employed to evaluate the overall voltage profile performance of the network. The VDI quantifies the deviation of bus voltages from the nominal value and serves as an important performance indicator for assessing voltage quality within the system. The Voltage Deviation Index is expressed as Equation 26: [22, 25]

$$VDI = \sum_{i=1}^{N} |V_i - 1| \quad (26)$$

Where VDI is the Voltage Deviation Index, V_i is the voltage magnitude at bus i (p.u.), N is the total number of buses in the system
A lower VDI value indicates a better voltage profile and improved system operating condition. Consequently, one of the objectives of the proposed optimization framework is to minimize the VDI while maintaining all bus voltages within the acceptable operating range. The minimum voltage stability margin of the network was further evaluated using the maximum FVSI value among all transmission lines. The system stability margin can be represented as Equation 27:

$$VSM = 1 - BVSI_{\max} \quad (27)$$

where VSM is the Voltage Stability Margin, $BVSI_{\max}$ is the maximum Bus Voltage Stability Index in the network A larger voltage stability margin indicates a more secure operating condition, whereas a smaller margin suggests that the system is operating closer to voltage collapse.

2.4 Implementation of Mayfly Optimization Algorithm

In this study, the Mayfly Optimization Algorithm (MOA) was employed to determine the optimal locations and capacities of photovoltaic (PV) and wind generation units within the IEEE 30-Bus transmission system. The optimization process aimed to minimize transmission power losses, reduce voltage deviations, and improve voltage stability margins while satisfying operational constraints.

2.4.1 Objective function

The quality of each candidate solution was evaluated using a multi-objective fitness function. The fitness function combines power loss minimization, voltage deviation reduction, and BVSI enhancement. The objective function is defined as Equation 28:

$$F = \omega_1 P_{loss} + \omega_2 VDI + \omega_3 BVSI_{\max} \quad (28)$$

where F is the overall fitness value, P_{loss} is the total real power loss, VDI is the Voltage Deviation Index, $BVSI_{\max}$ is the maximum Bus Voltage Stability Index, $\omega_1, \omega_2, \omega_3$ are weighting coefficients, in which $\omega_1 + \omega_2 + \omega_3 = 1$, and $(\omega_1 = 0.5, \omega_2 = 0.3, \omega_3 = 0.2)$ The optimization objective is to minimize the fitness function while satisfying network operational constraints.
The objective function was subjected to the following operational constraints:

i. Bus Voltage Constraints as given in Equation 10,
ii. Renewable Generation Capacity Constraints as given in Equations 29 and 30:

$$P_{PV}^{\min} \le P_{PV} \le P_{PV}^{\max} \quad (29)$$

$$P_{WG}^{\min} \le P_{WGV} \le P_{WG}^{\max} \quad (30)$$

where P_{PV} is the active power generated by solar PV energy, $P_{PV}^{\min}$ and $P_{PV}^{\max}$ are minimum and maximum active power generated by solar PV energy, P_{WG} is the active power generated by wind generator energy, $P_{WG}^{\min}$ and $P_{WG}^{\max}$ are minimum and maximum active power generated by wind generator energy,

iii. Generator Reactive Power Constraints as given in Equation 31:

$$Q_g^{\min} \le Q_g \le Q_g^{\max} \quad (31)$$

Q_g is the system reactive power generated, $Q_g^{\min}$ and $Q_g^{\max}$ are the system minimum and maximum reactive power generated

iv. Transmission Line Loading Constraints as given in Equation 32:

$$S_{line} \le S_{line}^{\max} \quad (32)$$

where S_{line} is the apparent power flow through the transmission line, $S_{line}^{\max}$ is the maximum thermal capacity of the transmission line.

2.4.2 MOA procedure

Each mayfly in the population represents a candidate solution containing the location and size of renewable energy generation units (PV and wind generator) to be integrated into the network. The optimization process begins by randomly generating a population of male and female mayflies within the feasible search space. Each mayfly was represented as a potential solution vector expressed as Equation 33:

$$X_i = \left[B_{PV}, P_{PV}, B_{WG}, P_{WG}\right] \quad 33$$

where B_{PV} is the location of photovoltaic generator, P_{PV} is the capacity of PV generator, B_{WG} is the location of wind generator, P_{WG} is the capacity of wind generator.

The initial population was generated within predefined limits corresponding to permissible bus locations and renewable energy capacities. According by [7], the movement of male mayflies is influenced by their individual best positions and the global best solution found by the swarm. Thus, for male mayflies, the optimization velocity was updated using Equation 34:

$$v_{ij}^{t+1} = gv_{ij}^{t} + a_1 e^{-\beta r_p^2}\left(pbest_{ij} - x_{ij}^{t}\right) + a_2 e^{-\beta r_g^2}\left(gbest_{ij} - x_{ij}^{t}\right) \quad 34$$

where v_{ij}^{t} is the current velocity of mayfly i, g is the gravity coefficient, a_1, a_2 are attraction coefficients, β is the visibility coefficient, r_p is the distance from personal best position, r_g is the distance from global best position, $Pbest$ is the personal best solution, $gbest$ is the global best solution

Also, the optimization position was updated using Equation 35:

$$x_i^{t+1} = x_i^{t} + v_i^{t+1} \quad 35$$

where; x_i^{t} is the current position, x_i^{t+1} is the updated position, v_i^{t+1} is the velocity of a male mayfly. This mechanism enables male mayflies to explore the search space and converge toward promising regions containing optimal solutions.

Also, the female mayflies are attracted toward male mayflies with better fitness values [7]. Their movement is governed by Equation 36:

$$v_{ij}^{t+1} = gv_{ij}^{t} + a_3 e^{-\beta r_{mf}^2}\left(x_{mj}^{t} - x_{ij}^{t}\right) \quad 38$$

where a_3 is the attraction coefficient, r_{mf} is the distance between male and female mayflies, x_{mj} is the position of the corresponding male mayfly.

The female mayflies position was updated using Equation 37:

$$y_i^{t+1} = y_i^{t} + v_i^{t+1} \quad 37$$

where y_{ji}^{t} is the current position , y_{ij}^{t+1} is the updated position obtained by adding velocity with current position. This attraction mechanism increases exploitation capability and enhances convergence toward high-quality solutions.

After movement updates, male and female mayflies mate to generate offspring solutions. The crossover operation was performed using Equations 38 and 39:

$$offspring1 = a_3 \times P_1 + (1 - a_3) \times P_2 \quad 38$$

$$offspring2 = (1 - a_3) \times P_1 + a_3 \times P_2 \quad 39$$

where P_1 represent male adults mayfly P_2, is the female adult mayfly

To prevent premature convergence and improve diversity, a mutation operation was applied to selected offspring according to Equation 40:

$$X_{new} = X_{old} + \sigma N(0,1) \quad 40$$

where σ is the mutation coefficient, $N(0,1)$ is the standard Gaussian random variable.

Mutation enables the algorithm to escape local optima and explore unexplored regions of the search space. Following mating and mutation, parent and offspring populations are merged and ranked according to fitness values. The best-performing individuals are selected to form the population for the next iteration. This elitism strategy ensures preservation of high-quality solutions throughout the optimization process.

The MOA was implemented in MATLABR2023a and integrated with MATPOWER for repeated load flow computations during the optimization process. The critical buses with binary value of one based on the

objective function (fitness value) were ranked as the most critical bus in the system. The new bus voltage, system current, active power loss and reactive power capacity in the power system were computed to meet the system load demands.

The stepwise for the simulation of the MOA based BVSI are follows:

Step 1:System data such as generation and load data were inputted;

Step 2 The population of the male and female mayflies is initialize and their velocity are determined;

Step 3: Iteration count was set to 1 (i=1) and the stability of the power system at contingency (20% increase in active and reactive power demands) operating condition was monitored using Equations 41 and 42 The proportional increase was applied to represent a stressed loading condition while preserving the original load power factor of the buses. The contingency was introduced to examine the response of the network to increased apparent-power demand and determine the resulting effects on bus voltage magnitudes, current levels, and voltage stability.

$$P_{L,i}^{cont} = 1.20 \cdot P_{L.i}^{base} \quad 41$$

$$Q_{L,i}^{cont} = 1.20 \cdot Q_{L.i}^{base} \quad 42$$

where $P_{L,i}^{base}$ and $Q_{L,i}^{base}$ are the base-case active and reactive power demands at bus i, respectively, while $P_{L,i}^{cont}$ and $Q_{L,i}^{cont}$ represent their corresponding values under the 20% loading contingency.

Step 4: Critical load bus was selected for any bus has value of BVSI higher than 0.5;

Step 5: The fitness value of MOA was evaluated using Equation 28

Step 6: The convergence (severity order of the selected critical buses) based on fitness value were checked (matting), if the bus fitness value less than one (1), iteration count were resect by 1 and step 4 was repeated, otherwise, the iteration was move to step 7;

Step 7: The new offspring were obtained using Equations 38 and 39;

Step 8: The worst mayflies were replaced with the best fitness value (new generation location);

Step 9: Best solution were displayed after replacing, and the process was stop.

2.5 Integration of PV and Wind Generators into the Transmission Network

The PV and wind generation units were incorporated into the IEEE 30-bus transmission system to evaluate their impact on voltage stability and overall network performance. The integration process was performed through the optimal placement and sizing framework developed using the MOA based BVSI. The PV and wind generator of unity power factor was employed as compensator device to inject active power at the selected buses and their effects on voltage stability are subsequently evaluated.

For grid-connected renewable generators equipped with PV and wind generator sources as shown in Figure 3. The PV and wind generation units were modelled as active power injection sources connected to selected load buses within the IEEE 30-bus system. The output power of the PV generator was represented as a function of solar irradiance and cell temperature. The generated power is expressed as Equation 43:

$$P_{PV} = P_{rated}\left(\frac{G}{G_{ref}}\right)\cdot\left(1+\alpha\left(T_c - T_{ref}\right)\right) \quad 43$$

where P_{PV} is the power generated by solar energy, P_{rated} is the rated PV power, G is the incident solar irradiance, G_{ref} is the reference irradiance, α is the temperature coefficient, T_c is the cell temperature, T_{ref} is the reference temperature.

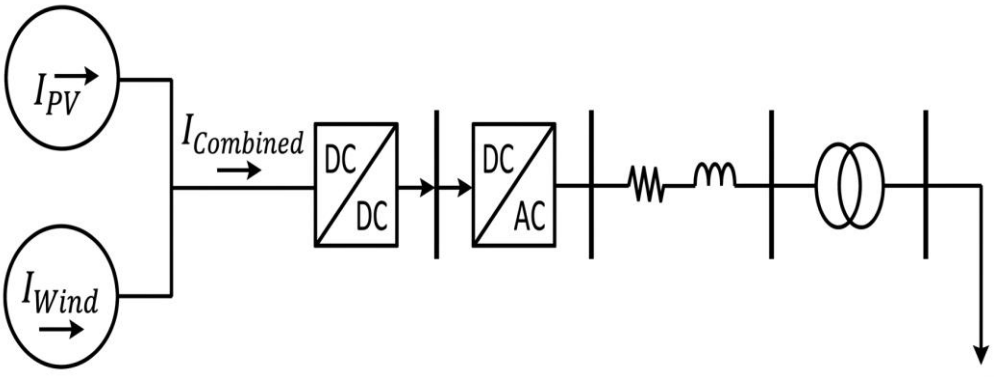


Figure 3: Grid-Connected Renewable Generators with PV and Wind Generator

The wind turbine output power was modelled using the wind speed-power relationship expressed as Equation 44:

$$P_{WG} = N_{wt} * \begin{cases} 0 \; if \; V < V_c, V > V_f \\ P_r * \frac{(V - V_c)}{(V_r - V_c)} \; if \; V_c \leq V \leq V_r \\ P_r \; if \; V_r \leq V \leq V_f \end{cases} \quad 44$$

where; V_1 is the peed at the hub height (H_1), V is the speed at the reference height (H), a is the friction coefficient, P_r is rates power, V_r, is rated speed characteristics, V_c is cut-in speed. V_f is cut-off, N_{wt} is the number of wind turbines, and P_{wt} is the wind generator rated power (kW).

The integration of renewable generators modifies the power balance equations by introducing additional active power generation at the connected buses. Consequently, the net active and reactive power demand at a bus is expressed as Equations 45 and 46:

$$P_{Gi}^{new} = P_{Gi} + P_{PV} + P_{WG} \quad 45$$

$$Q_{Gi}^{new} = Q_{Gi} + Q_{PV} + Q_{WG} \quad 46$$

where P_{Gi}^{new} is the new generated active power at bus i, P_{Gi} is the conventional generator power at bus i, P_{PV} is the active power supplied by the Solar PV generator, and P_{WG} is the active power supplied by the wind generator., Q_{Gi}^{new} is the total reactive power generation at bus i, Q_{Gi} is the reactive power supplied by the conventional generator at bus i, Q_{PV} and Q_{WG} represent the reactive power contributions from the PV and wind generators respectively.

The active and reactive power balance Equation for each bus in the transmission network after RES integration was represented as Equations 47 and 48:

$$P_{Gi}^{new} - P_{Di} = \sum_{j=1}^{N} |V_i||V_j||Y_{ij}| \cos\left(\theta_{ij} + \delta_j - \delta_i\right) \quad 47$$

$$Q_{Gi}^{new} - Q_{Di} = \sum_{j=1}^{N} |V_i||V_j||Y_{ij}| \sin\left(\theta_{ij} + \delta_j - \delta_i\right) \quad 48$$

where P_{Di} and Q_{Di} are the active and reactive power demands at bus i, V_i and V_j are the bus voltage magnitudes, Y_{ij} is the bus admittance matrix element, and δ_j and δ_i are the bus voltage phase angles.

After the integration of the PV and wind generators, the Newton-Raphson load flow analysis was repeated to evaluate the post-integration voltage stability performance of the transmission network. The simulation was carried out in MATLAB R2023a, and the resulting voltage magnitudes, BVSI values, and active power losses were compared with the pre-integration results to assess the effectiveness of the RES placement.

2.6 Comparison of the Approaches

The results of application of NOA based BVSI for determination of the PV and wind generator location were compared with Line Stability Index (LSI) and Equilibrium Optimizer (EO) algorithm. The comparison was based on the common objective of identifying voltage-critical buses under contingency conditions and evaluating their suitability for corrective renewable-energy integration. The LSI was selected as a conventional voltage-stability benchmark because it quantitatively indicates the severity of voltage instability, with values approaching unity representing increased vulnerability. The EO was selected as an optimisation benchmark because it is a population-based metaheuristic capable of ranking candidate buses using a fitness function. For consistency, MOA based BVSI, LSI and EO were evaluated on the same IEEE 30-bus network under the same contingency condition using NR load-flow results. The approaches were compared based on critical-bus identification, bus voltage magnitude, system current, active power loss and the provision of targeted corrective locations.

The Line Stability Index (LSI) of voltage stability technique was used to determine the severity order of the selected critical load bus in the IEEE 30-bus power system during contingency. The LSI was computed based on objective function in Equation 28 using Equation 49 [4]:

$$LSI = \frac{4XQ_r}{|V_s|^2 Sin^2(\theta - \delta)} \leq 1 \quad 49$$

where; Q_r is reactive power load at receiving-end, θ is the voltage phase angle difference, X is the transmission line reactance, V_s is the sending-end voltage, δ is a voltage phase angle. The load bus with value of LSI very closed to one was selected as most critical load bus of the power system.

Similarly, Equilibrium optimizer (EO) was employed as optimization technique to determine the severity order of the selected critical buses during the contingency on IEEE 30-bus system. The EO optimally rearranges the critical load bus based on their severity order (fitness function) in the power system. The EO algorithm was implemented and a random population was determined. The EO particles was evaluated using fitness function in Equation 48 and each particle of EO was updated using Equations 50.

$$FF = optimize\sum_{i=1}^{N} f(x_i) \quad 50$$

where; FF is the fitness function, f is objective function, N is the number of the bus, x is the vector of variable or particles of the critical buses.

Then, each particle of EO was updated using Equations 51 to 53 [1].

$$C_{eq.pool} = \{C_{eq(1)}, C_{eq(2)}, C_{eq(3)}, C_{eq(4)}, C_{eq(ave)}\} \quad 51$$

$$\overrightarrow{F} = a_1 \sin\left(\vec{r} - 0.5\right) \cdot [e^{-\vec{\lambda}t} - 1] \quad 52$$

$$\vec{G}_0 = \overrightarrow{GCP}\left(\vec{C}_{eq} - \vec{\lambda}\vec{C}\right) \quad 53$$

where; $C_{eq.pool}$ equilibrium pool, C_{eq} is the concentration of particles inside the control volume at an equilibrium state without generation, F is velocity term function, G_0 is the initial value and k is a decay constant (k=λ), ; λ is a random vector between the interval [0, 1],, GCP is generation rate control parameter; r are random numbers between [0, 1], and C is the concentration within the control volume

The particles (load bus) were evaluated for their fitness function and each particle update its concentration based on the fitness value in Equation 30. The EO search agents randomly update its concentration with respect to best solutions to the final equilibrium state.

2.7 Simulation Procedure and Implementation in MATLAB R2023a

The simulation and optimization processes developed in this study were implemented in MATLAB R2023a using the MATPOWER toolbox. MATLAB R2023a was selected because of its robust computational capabilities, extensive numerical analysis libraries, and compatibility with power system simulation tools. MATPOWER provides a flexible platform for performing power flow analysis, optimal power flow studies, and power system optimization, making it suitable for implementing the proposed MOA-based BVSI renewable energy integration framework. The IEEE 30-Bus test system was imported into the MATLAB environment using the standard MATPOWER case file (case30.m). The flowchart algorithm algorithm for the detail simulation is shown in Figure 4.

The flowchart summarises the simulation procedure used to evaluate and compare the MOA-based BVSI, LSI, and EO approaches on the IEEE 30-bus transmission system. The process begins by inputting the network, load, generator, line, and renewable-energy constraint data, followed by Newton–Raphson load-flow analysis to determine the initial system operating condition. The three approaches are then applied to identify and rank weak or critical buses and determine suitable locations and sizes for PV and wind generation units. After renewable-energy integration, the load flow was repeated to evaluate voltage profile, power losses, and voltage-stability indices. The convergence criterion is checked, and the optimisation process is repeated when it is not satisfied. Finally, the results obtained using MOA-based BVSI, LSI, and EO are compared, and the optimal buses, renewable-energy sizes, voltage profile, power losses, and stability performance are presented as the simulation outputs.

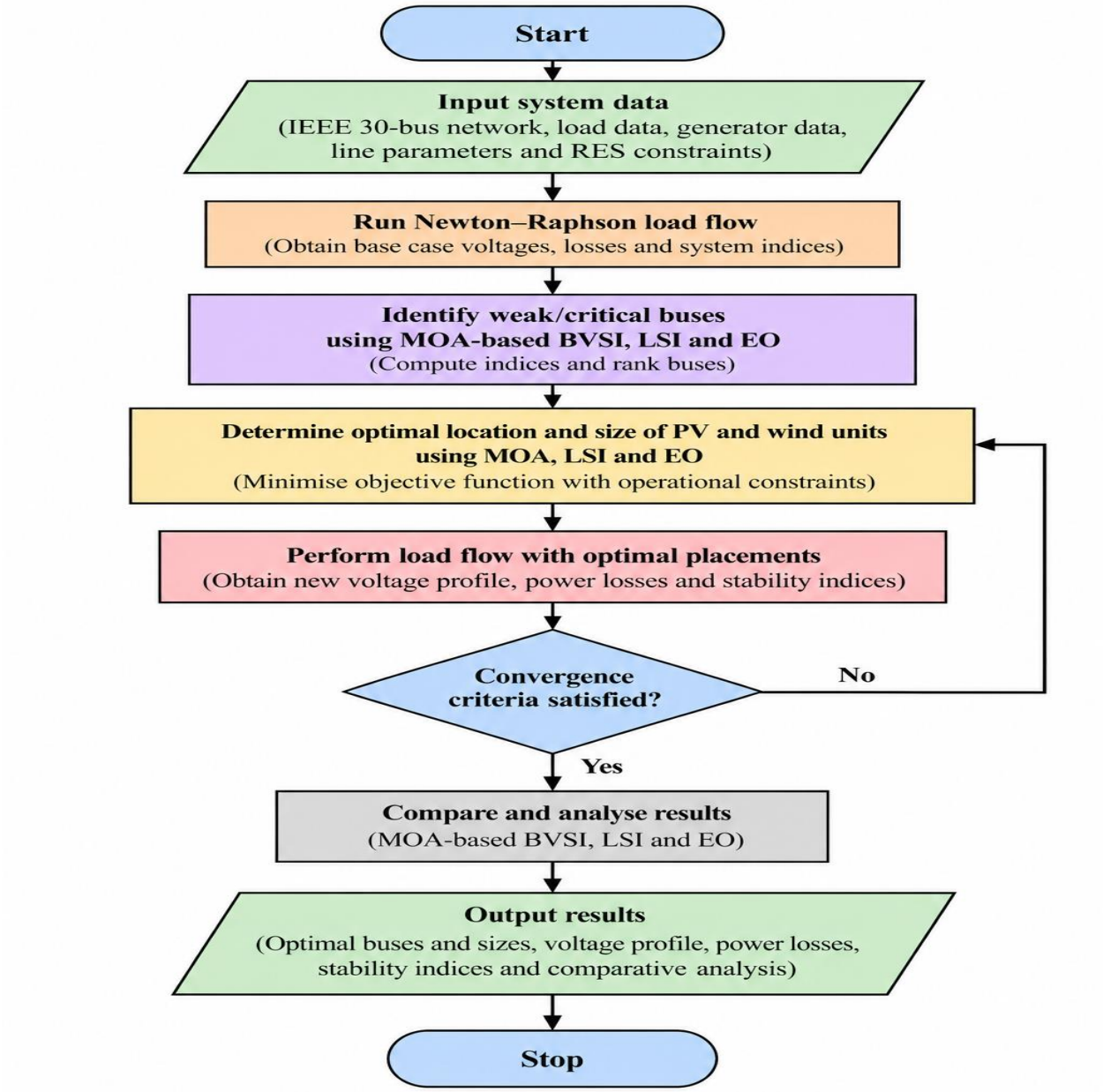


Figure 4: Flowchart Algorithm for the Comparison of the Approaches

3. RESULTS AND DISCUSSION

Table 3 presents the steady-state load-flow results of the IEEE 30-bus test system. The obtained bus-voltage magnitudes range from 0.936 p.u. to 1.057 p.u. relative to the adopted acceptable operating range of 0.95–1.05 p.u. Although most buses operate within the specified limits, bus 5 records a minimum voltage magnitude of 0.936 p.u., indicating an undervoltage condition, while bus 23 records 1.057 p.u., slightly exceeding the upper voltage limit and indicating an overvoltage condition. The voltage magnitudes specified for the generator (PV) buses correspond to their adopted voltage set-points and are not necessarily equal to 1.0 p.u. These results indicate that the base-case network is generally within the prescribed voltage range at most buses, although the identified voltage-limit violations require appropriate corrective voltage-control measures. Also, the bus-voltage angles vary smoothly from 0 degree at the swing bus to 3.45° at bus 21. This progressive angular rise reflects an efficient real-power transfer from the generation sources to the load centers. The absence of abrupt phase-angle deviations confirms that the system experiences no significant congestion, line overload, or reactive-power stress under the steady-state scenario. This was also confirmed by Biswal and Shankar (2022) and Yang *et al.* (2024). In addition, the analysis reveals that the total active power losses in the system are approximately 324.31 MW, whereas the total reactive power losses amount to 228.85 MVAr. The higher value of active-power loss indicates that a considerable portion of generated power is dissipated as heat through transmission lines due to their inherent resistance. In contrast, the reactive-power loss represents energy oscillations associated with magnetic and electric field exchanges

within the lines and transformers. This was also confirmed by Biswal and Shankar (2022) and Yang *et al.* (2024).

Table 3: Steady State Load Flow Results of IEE 30-Bus System

Bus No	Bus Type	Voltage Magnitude (p.u)	Voltage Angle (Degree)	Load (MW)	Load (MVAr)
1	Swing	1.0000	0.0000	0	0
2	PV	0.9630	1.5160	21.7	12.9
3	PQ	0.9780	1.6270	2.4	1.2
4	PQ	1.0240	0.6750	7.6	1.6
5	PQ	0.9360	1.6700	0	0
6	PQ	1.0210	2.9380	0	0
7	PQ	0.9970	1.9510	22.8	7.9
8	PQ	1.0160	1.9530	30	30
9	PQ	0.9830	1.9520	0	0
10	PQ	0.9930	0.9360	5.9	2
11	PQ	1.0320	1.1170	0	0
12	PQ	1.0130	0.4970	11.2	7.5
13	PQ	1.0410	2.4740	0	0
14	PQ	1.0290	2.8950	6.2	1.6
15	PQ	1.0370	2.5940	8.4	2.5
16	PQ	1.0150	0.5880	3.5	1.8
17	PV	0.9820	2.5440	9	4.8
18	PQ	1.0220	2.9100	3.2	0.9
19	PQ	0.9950	0.6270	9.5	3.4
20	PQ	0.9910	0.5990	4.2	0.7
21	PQ	0.9890	3.4470	19.7	5.2
22	PQ	0.9880	2.4370	0	0
23	PQ	1.0570	1.4210	3.2	1.6
24	PQ	0.9630	1.3450	18	5.7
25	PQ	0.9580	1.3660	1	0
26	PQ	1.0290	3.4320	2.5	2.3
27	PQ	1.0250	0.6320	0	0
28	PQ	1.0130	2.4520	0	0
29	PQ	0.9980	2.0770	3.7	0.9
30	PV	0.9940	1.0370	12	1.9
Total Power Losses				324.31 MW	228.85 MVAr.

Figure 5 depicts the variation of the BVSI across all buses of the IEEE 30-bus system at contingency. The BVSI provides a quantitative indication of each bus's proximity to voltage instability smaller values denote a healthy voltage-stability margin, while values approaching or exceeding 0.45 signal potential weakness or risk of collapse. A general upward trend in BVSI values is observed compared with the steady-state case, confirming that the increased load has stressed the network and reduced its voltage-stability margin. Most buses still maintain BVSI values below 0.45, showing that they remain stable even under higher reactive-

power demand. However, buses 5, 7, 16, 19 and 23 recorded BVSI values above this critical threshold. These buses are therefore identified as voltage-stability-violating points or critical buses that require attention.

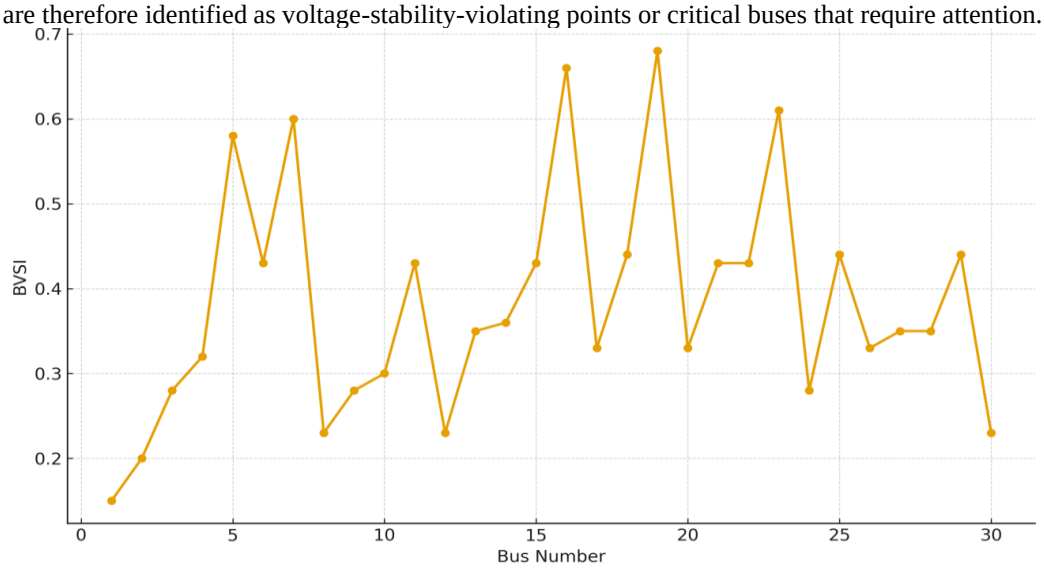


Figure 5: BVSI and Bus Number of IEEE 30-Bus System at Contingency

Table 4 present the contingency load-flow results for selected buses 5, 7, 16, 19, and 23 of the IEEE 30-bus system following a 20 % increase loading condition. These buses were chosen because they had previously been identified as critical buses based on their BVSI values exceeding the threshold of 0.45 in Figure 5. This was done to evaluate how the increased loading affects the load buses voltage magnitudes and current levels, and to determine the degree of voltage stress in each bus. The results shows that the bus-voltage magnitudes range from 0.9201 p.u to 0.9430 p.u, which indicates that all selected buses experience voltage deviations below the standard limit of 0.95 p.u. This voltage drop signifies that the system has entered a region of reduced voltage stability due to the extra reactive-power loading. Among the selected buses, bus 23 recorded the lowest voltage magnitude (0.9201 p.u), indicating that it is the most voltage-stressed bus in the network. The current magnitudes for the selected buses range between 15.146 p.u and 24.714 p.u, demonstrating a significant rise in current flow compared with steady-state operation.

Table 4: Voltage and Current Magnitude of Selected Buses of IEEE 30-Bus at Contingency

Bus No	Voltage Magnitude (p.u)	Current Magnitude (p.u)
5	0.9310	24.714
7	0.9430	15.221
16	0.9320	15.146
19	0.9341	15.596
23	0.9201	17.253

Figure 6 illustrates the total active and reactive power losses obtained from the load-flow analysis of the IEEE 30-bus transmission system under contingency conditions, where the reactive load on all buses was increased by 20 %. The Figure presents a comparison between active power losses (MW) and reactive power losses (MVAr) to assess how network stress influences system efficiency and voltage stability. The results show that the active power loss increased significantly to 453.06 MW, while the reactive power loss rose to 329.85 MVAr. This notable rise in both parameters compared with the steady-state values (324.31 MW and 228.85 MVAr, respectively) demonstrates that system losses increase sharply with higher loading conditions
Figure 7 presents the MOA fitness profile for the IEEE 30-bus transmission system. The plotted fitness pattern shows that buses 5, 16, and 23 attained the maximum fitness value of 1.0, indicating that the MOA algorithm consistently classified these buses as the weakest nodes in the network. Their elevated fitness values directly imply that these buses should receive priority attention during stability improvement, optimal DG placement, or reactive-power support planning. These buses are likely located along long, high-impedance corridors or areas with concentrated load, making them more vulnerable to voltage depression and reactive-power imbalance. In addition to these three most critical buses, the algorithm assigned relatively high fitness values to buses 7, 19, 24, 26, and 29, each recording fitness values between 0.28 and 0.46.

Although these buses are not as weak as the top-ranked critical nodes, their moderate fitness magnitudes indicate that they experience noticeable voltage stress and could become unstable under more severe contingencies. These buses therefore constitute the secondary priority group for corrective actions such as capacitor placement, OLTC adjustments, or reinforcement of local distribution corridors.

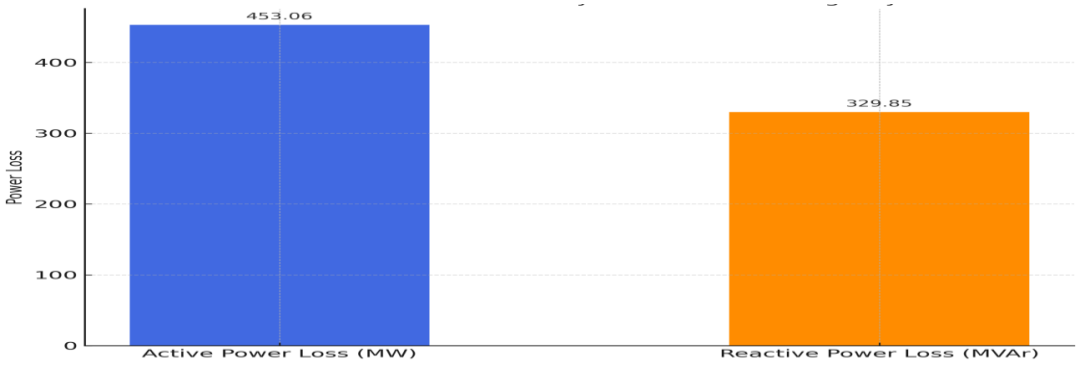


Figure 6: Total Power Losses of IEEE 30-Bus at Contingency

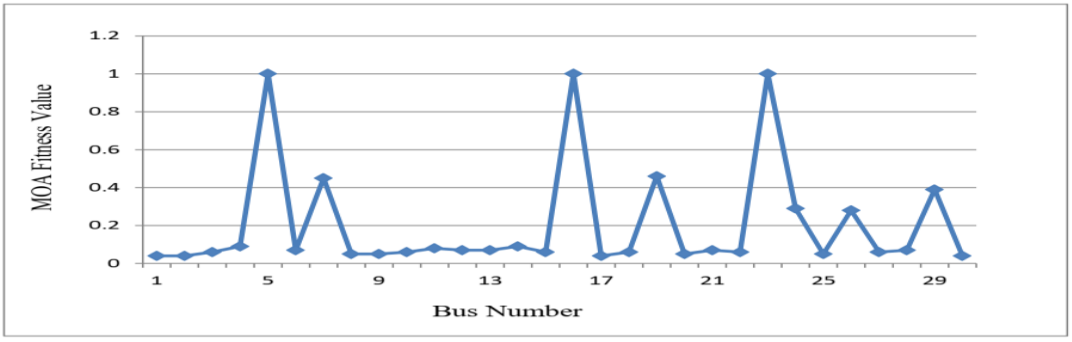


Figure 7: MOA Fitness Value and Bus Number of IEEE 30-Bus System at Contingency

Table 5 presents the contingency load-flow results for selected buses 5, 16, and 23 of the IEEE 30-bus system with MOA. These buses were selected because they achieved a binary fitness value of 1, meaning MOA ranked them as the weakest locations in the network where voltage instability is most likely to occur under stressed loading conditions. Under contingency conditions, all three buses experience notable voltage depression, with voltage magnitudes ranging from 0.9502 p.u to 0.9550 p.u. Although these values remain within the acceptable operational band, they are positioned very close to the lower stability margin, confirming their vulnerability. Among them, bus 16 shows the lowest voltage (0.9502 p.u), indicating that it is the most stressed in terms of voltage support. This agrees with its MOA fitness ranking, reinforcing that the algorithm accurately detects points of reduced reactive-power strength in the system. The current magnitudes recorded at the three buses provide further insight into their operating stress levels. bus 5 exhibits a very high current magnitude of 20.012 p.u, which is consistent with its heavy loading and confirms its role as a major power-transfer corridor during contingency

Table 5: Load Flow Result of Selected Buses of IEEE 30-Bus with MOA

Bus No	Voltage Magnitude (p.u)	Load (MW)	Load (MVar)	Current Magnitude (p.u)
5	0.9520	2.11	0.70	20.012
16	0.9502	0.75	0.35	9.406
23	0.9550	0.88	0.43	14.750

Figure 8 presents the total active and reactive power losses for the IEEE 30-bus transmission system after applying the MOA under contingency conditions. The objective of the MOA in this stage is to enhance the network's performance by optimally identifying and correcting the most critical buses, thereby reducing the stress imposed on the system during high-loading or disturbed scenarios. Under contingency, the network's active power loss is reduced to 338.10 MW, and the reactive power loss is reduced to 257.60 MVAr. These

results represent a significant improvement compared to the earlier contingency case without optimization, where the system recorded 453.06 MW and 329.85 MVAr, respectively.

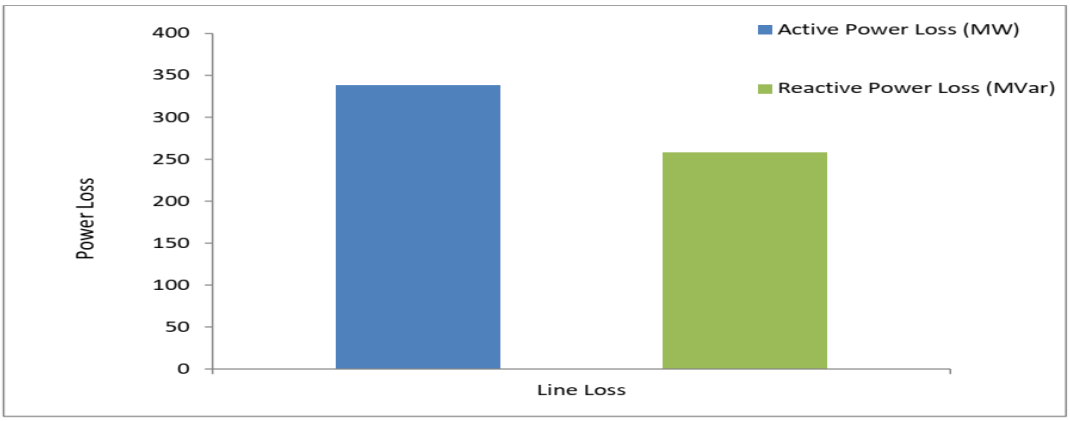


Figure 8: Total Power Losses of IEEE 30-Bus at Contingency with MOA

Table 6 presents the performance improvement achieved in the IEEE 30-bus system after installing inverter-based PV and wind generators at the three most critical buses 5, 16, and 23 as identified by MOA. The table compares the resulting voltage magnitudes, current magnitudes, and MVar injection levels for both PV-based and wind-based compensation strategies. From the Table, the appropriate PV and wind generator sizes of (0.36, 0.27 and 0.27 MVar) and (0.24, 0.18 and 0.18 MVar) were place at the selected buses 5, 16 and 23, respectively. This proportional allocation demonstrates that Var support targeted according to MOA fitness ranking is highly effective, as the weakest buses experienced the greatest improvement. The results show that the integration of PV generators significantly improved the bus voltage profiles, with all three selected buses attaining a voltage magnitude of **1.0000 p.u.** This improvement is attributed to adequate solar irradiance, which enabled sufficient PV power generation to support the local load demand and reduce voltage drops within the network, thereby restoring the bus voltages to their nominal values. The associated current magnitudes also decreased to 16.874, 6.001 and 12.980 p.u, demonstrating that the additional reactive power reduced line loading and minimized the stress on nodes. even under contingency, reflecting improved hosting capability. The wind generator contributions similarly improved voltage stability but produced slightly lower voltage recovery compared to PV. Under wind integration, buses 5, 16 and 23 have voltage magnitude value of 0.9870, 1.0000 and 0.9901 p.u,, respectively, which are within acceptable limits but not achieving the full 1.0000 p.u restoration observed with PV. This difference is expected because the assigned reactive-power injection from wind (0.18–0.24 MVar) was lower than that of PV (0.27–0.36 MVar),

Table 6: Improvement of IEEE 30-bus system with PV and Wind Generator

	With PV Generator			With Wind Generator		
Bus No	Voltage Magnitude (p.u)	Current Magnitude (p.u)	Size (MVar)	Voltage Magnitude (p.u)	Current Magnitude (p.u)	Size (MVar)
5	1.0000	16.874	0.36	0.9870	16.367	0.24
16	1.0000	6.001	0.27	1.0000	5.904	0.18
23	1.0000	12.980	0.27	0.9901	12.732	0.18

Figure 9 illustrates the variation in total active power loss of the IEEE 30-bus system with integration of PV and with wind generator. The results highlight how system stress, optimization strategies, and renewable-energy integration influence transmission efficiency and power-loss behaviour. It could be observed that when PV generators are integrated at the MOA-identified critical buses, the total active power loss reduces drastically to 256.40 MW, compared with steady state, contingency and with MOA values of 324.31, 453.06 and 338.10 MW respectively. This outcome demonstrates the strong voltage-support capability of PV inverters, which can supply fast, controllable Var that significantly strengthen weak voltage buses. Integration of wind generators also improves system performance, yielding a reduced active power loss of 283.77 MW. The wind-based compensation delivers substantial improvement compared to both steady-state and contingency value of 324.31 and 453.06 MW. The reduction in power loss confirms that renewable-energy can serve as effective reactive-power compensators in modern power systems.

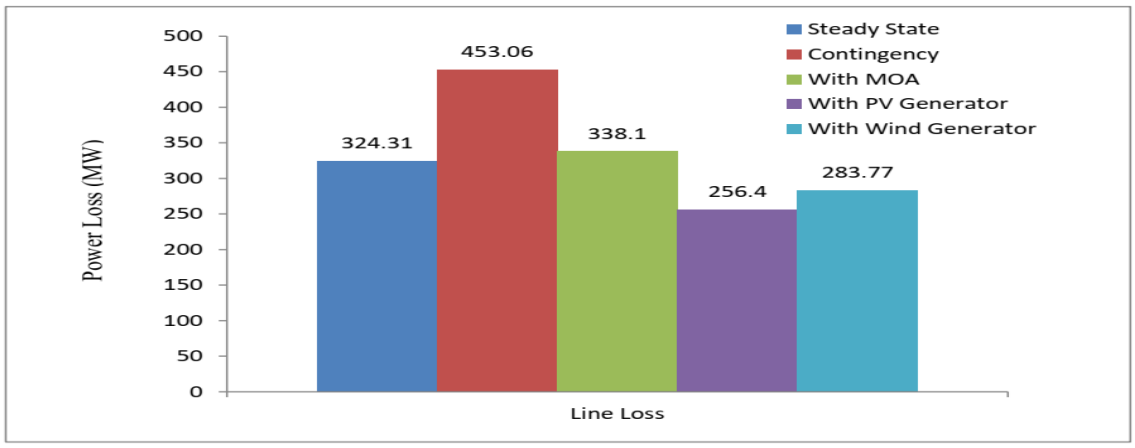


Figure 9: Total Active Power Loss of IEEE 30-Bus System with PV and Wind Generator

Figure 10 presents a comparative analysis of the voltage magnitudes across the IEEE 30-bus system under contingency conditions using three techniques; MOA based BVSI, LSI, and EO. The MOA based BVSI approach identified Buses 5, 16, and 23 as the most voltage-sensitive locations for the optimal placement of PV and wind generators, with voltage magnitudes of 0.9520, 0.9502, and 0.9550 p.u, respectively. Under the EO technique, the buses selected for generator placement shifted to Buses 5, 7, and 19, each exhibiting the same voltage magnitude of 0.9500 p.u. This consistency suggests that EO identifies a different set of weak buses based strictly on its optimization criterion. In contrast, the LSI method classified almost all load buses as critical, implying a lack of selectivity and an overestimation of system vulnerability.

The comparison across the three techniques reveals important differences. Both the MOA based BVSI and EO algorithm produce results that fall within the ±5% voltage tolerance margin, meaning their selected buses meet the acceptable steady-state voltage criteria. However, the results generated by LSI show that many buses fall outside the allowable voltage range, incorrectly suggesting widespread instability. This occurs because LSI responds strongly to minor variations in loading, causing many buses to appear unstable even when their voltages remain within acceptable limits. Overall, MOA based BVSI and EO provide more focused and realistic identification of vulnerable buses, whereas LSI-based lack accuracy and discriminate poorly between stable and unstable buses.

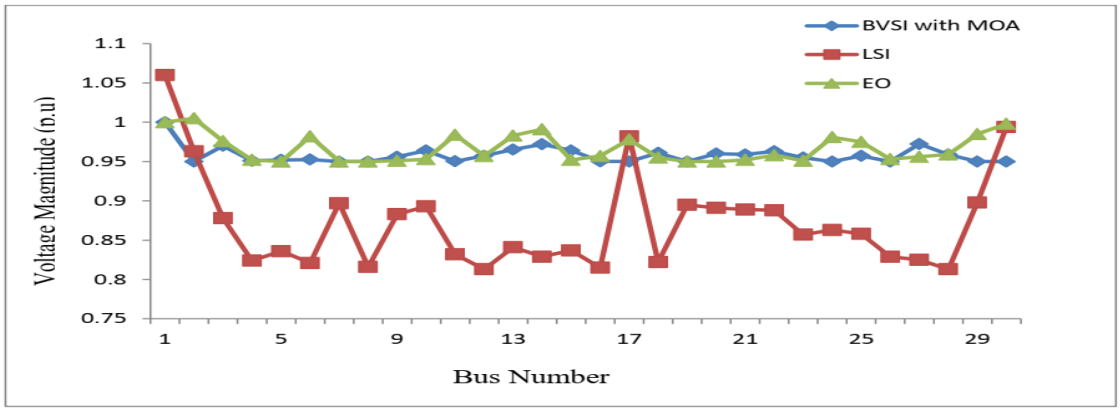


Figure 10 Comparison of Voltage Magnitude of IEEE 30-Bus System at Contingency

Figure 11 compares the total active power losses obtained using the MOA based BVSI, LSI, and EO techniques under contingency conditions in the IEEE 30-bus transmission system. The differences in the loss values directly reflect how effectively each method identifies and strengthens the critical buses responsible for voltage instability and excessive line loading. The MOA based BVSI technique produces the lowest power loss of 338.10 MW, indicating superior performance in mitigating system stress during contingency. This is because the MOA-based BVSI combines voltage-stability assessment with the optimisation process to identify and rank the most critical buses, thereby prioritising these locations for the optimal placement of PV and wind generation units to improve bus voltage profiles, enhance voltage stability, and reduce transmission power losses. The EO technique also reduced the active power loss to 340.02 MW. However, the EO implementation ranks candidate buses according to its defined fitness function without explicitly incorporating the BVSI-based voltage-stability sensitivity of each bus into the search process. Consequently, the buses selected by EO are determined primarily from the optimisation objective rather than their proximity to voltage instability. In contrast, the MOA-based BVSI framework incorporates the voltage-stability

condition of the buses into the optimisation process, allowing critical-bus identification and renewable-energy placement to consider both system performance and voltage-stability requirements.
In contrast, the LSI technique produces the highest loss: 418.04 MW, significantly larger than both BVSI-MOA and EO. This highlights a major limitation of LSI: it tends to identify a broad set of buses as unstable, leading to scattered and less targeted reinforcement. Because LSI lacks the discriminatory precision of BVSI-MOA, it does not effectively minimize current congestion in critical lines.

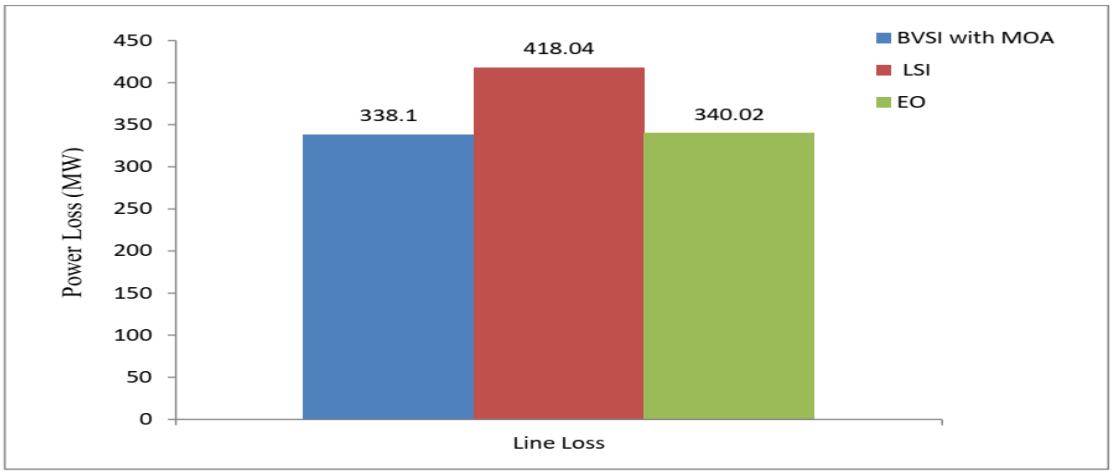


Figure 11 Comparison of Active Power Loss of IEEE 30-Bus System at Contingency

4. CONCLUSION

This study has successfully implemented a MOA-based framework for voltage stability enhancement and renewable energy integration in the IEEE 30-bus transmission system. The results demonstrated that increased reactive loading under contingency conditions significantly deteriorated system performance, leading to voltage depression and substantial increases in active and reactive power losses. Using the MOA based BVSI approach, buses 5, 16, and 23 were accurately identified as the most critical buses requiring corrective intervention. The application of MOA successfully reduced contingency active power losses from 453.06 MW to 338.10 MW while improving voltage stability margins. Furthermore, the optimal placement of inverter-based photovoltaic and wind generators at the identified buses provided additional performance improvements. PV integration produced the best results by restoring bus voltages to approximately 1.0 p.u. and reducing active power losses to 256.40 MW, while wind generator integration reduced losses to 283.77 MW and maintained acceptable voltage profiles. Comparative evaluation against EO and LSI techniques confirmed that the BVSI-MOA approach provides superior selectivity, better identification of vulnerable buses, and greater loss reduction capability. Therefore, the proposed methodology offers an effective tool for transmission network planning, voltage stability enhancement, and optimal deployment of renewable energy resources in modern power systems.

REFERENCES

[1] Abdel-Basset, M., Chang, V. and Mohamed, R. (2021). A novel equilibrium optimization algorithm for multi-thresholding image segmentation problems. *Neural Computer and Application*, **33:** 10685–10718.

[2] Abo-Elyousr, A. El-Hameed, M. and El-Saadawi, M. (2021). Optimal Distributed Generation Placement using Particle Swarm Optimization, *Electric Power Components and Systems*, 49(4): 345–357, 2021.

[3] Adebayo, I. G. and Sun, Y. (2022). New approaches for the identification of influential and critical nodes in an electric grid. *Archives of Electrical Engineering*, **71**(3): 671 –686.

[4] Adebayo, I. G., Jimoh, A. A., Yusuff, A. A. and Sun, Y. (2018). Alternative method for the identification of critical nodes leading to voltage instability in a power system. *African Journal of Science, Technology, Innovation and Developmen*t, 1(2): 1-22.

[5] Adetokun, B. B., Muriithi, C. M., Ojo, J. O. and Oghorada, O. (2023). Impact assessment of increasing renewable energy penetration on voltage instability tendencies of power system buses using a QV-based index. *Scientific Reports*, **3** (23) 13-22

[6] Ahiakwo, C. O., Braide, S. L. Amadi, H. N. and Ehimhen, E. A. (2024). Voltage stability prediction of Nigerian 330kv network using arithmetic moving average technique. American Journal of Engineering Research, 13(6): 111- 126,

[7] Amarendra, A, Kumar, P. and Singh, R. (2023). "Application of Mayfly Optimization Algorithm to Engineering Optimization Problems: A Review," *Applied Soft Computing*, 12(4): 109-124.

[8] Amosedinakarann, S., Mala, K., Bhuvanesh, A., Kannan, A. and Pandiyan M. K. (2021). Generation expansion planning for a real-world power system: aiming towards cost and environmental emission minimization by penetrating huge renewable energy sources *Journal of Electrical Engineering and Technology*, **16**(268): 2835-2846.

[9] Bello, M. M., Okafor, E. C. and Iyidobi, J. C. (2021). Improving Voltage Stability on the 46 Bus 330 kV Nigeria Transmission Network using ANFIS Controlled TCSC and SSSC. *International Research Journal of Applied Sciences, Engineering and Technology*, **7**(6): 56-64.

[10] Biswal, R. S. and Shankar, G. (2022). Optimal deployment and sizing of distributed generations and capacitor banks in radial distribution system using African vultures optimization algorithm. *3rd International Conference on Energy and Power, Bagdad*, 1-8.

[11] Bošnjakovi´c, M., Santa, R., Crnag, Z. and Bošnjakovi´c, D. (2023). Environmental Impact of PV Power Systems. *Sustainability*, 15 (23): 1-26

[12] Dodo U. A., Ashigwuike, E. C. and Eronu, E. M. (2021). Renewable energy readiness in Nigeria: a review focusing on power generation. *Uniabuja Journal of Engineering and Technology*, **1**(1): 115-144.

[13] Elgamal, Z. M., Yasin, N. N., Md-Sabri, A. Q., Sihwail, R., Tubishat, M. and Jarrah, H. (2021). Improved equilibrium optimization algorithm using elite opposition-based learning and new local search strategy for feature selection in medical datasets. computation, **9** (68): 1-23

[14] Faramarzi, A., Heidarinejad, M., Stephens, B. and MirjaliliS. (2019). Equilibrium optimizer: a novel optimization algorithm. knowledgebased systems, 105-109.

[15] Feng, N., Niu, T., Yan, J., Zhang, Y., Feng, Y., and Lei, Y. (2025). Optimal placement and sizing of reactive power compensation devices in power grids with high penetration of distributed generation. Processes, 13(9), 29-53.

[16] Gaho, Y., Zhou, Y. and Luo, Q. (2020). An efficient binary equilibrium optimizer algorithm for feature selection. digital object identifier, *Access*.2020.3013617

[17] Gandh, O., Kumar, D. S., Rodríguez-Gallegos, C. D., Srinivasan, D. (2020). Review of power system impacts at high PV penetration Part I: Factors limiting PV penetration. *Solar Energy* **210** (20) 181–201.

[18] Gao, Z. M., Zhao, J., Li, .R. and Hu, Y. R. (2020). The improved mayfly optimization algorithm for optimal power flow solutions and loss reduction. Journal of Physics Conference Series, 1684(20): 1-7

[19] Govil, V. K., Tripathi, S. M., and Sahay, K. (2025). Real-time assessment of PV-DSTATCOM for grid power quality enhancement using an indirect current-control strategy. Scientific Reports, 15(6).1598-1606

[20] Ismai, B., Wahab, N. A.,Othman, M. L., Radzi, M. A., Vijayakumar, K. N., Rahmat, M. K. and Matnaain, M. N. (2022). New line voltage stability index for voltage stability assessment in power system: the comparative studies. *IEEE Access, Digital Object Identifier* 1-10.

[21] Kumar P. and R. Rao, R (2023). Optimal Wind Generation Allocation using Whale Optimization Algorithm for Transmission Loss Reduction. *Energy Reports*, 9(2): 2150–2163

[22] Mahmoud, K. Abdel-Nasser, M. and Lehtonen, M. (2022). Hybrid GA-PSO Approach for Optimal Renewable Energy Allocation in Power Systems. *Sustainable Energy Technologies and Assessments*, 52(1): 102-120,

[23] Mamta, A. and Singh, B. (2020). Optimal Control of DC Motor using Equilibrium Optimization Algorithm. International Journal of Engineering Research and Technology, **9** (5): 1272-1275.

[24] Nguyen, N. A., Vo, D. N., Nguyen, T. T. and Duong, T. L. (2022). An improved equilibrium optimizer algorithm for solving optimal power flow problem with penetration of wind and solar energy *International Transactions on Electrical Energy Systems*, **22**: 12-21

[25] Nwafor, C, U. and Onu, C. (2022). Impact on power system collapse in Nigeria transmission networks with application of voltage stability indices. *International Journal of Frontiers in Engineering and Technology Research*, 3(1):1–9.

[26] Nwaigwe, R. N., Mutabilwa, P. and Dintwa, E. (2019). An overview of solar power (PV systems) integration into electricity grids. *Materials Science for Energy Technologies* 2 (19) 629–633

[27] Sule, A. H. (2022). Impact of Integration of Renewable energy sources on power system stability, fault protection and location: a review. *Direct Research Journal of Engineering and Information Technology*, 9 (4): 87-100.

[28] Yang, k. and Pan , D. (2023). An improved mayfly optimization a;gorithm for type 2 multi-objective integrated process planning and scheduling. Mathematics Journal , 11(20): 34-43.

[29] Yang, Q., Wang, J., Liang, J. and Wang, X. (2024). Chance-constrained coordinated generation and transmission expansion planning considering demand response and high penetration of renewable energy. *International Journal of Electrical Power and Energy Systems*, **155** (24) 1-15.

[30] Yunfei, D. Shen, X., Kammen, D. M., Hong, C., Nie, J., Zheng, B. and Yao, S. (2024). A generation and transmission expansion planning model for the electricity market with de-carbonization policies. *Advances in Applied Energy*, **13** (24): 1-18.

[31] Zervoudakis, K. and Tsafarakis, S. (2020). A mayfly optimization algorithm. *Computer and Industrial Engineering*, **35**(20): 1 -12.

[32] Zhang, L., Chen, Z., Zhang, H., Ma, Z., Caao, B. and Song, L. (2020). Accurate study and evaluation of small PV power generation system based on specific geographical location. *Journal of Energy Engineering*, **117**(16): 453- 470.